Energy-dissipation Mechanisms Associated with Rapid Fracture of Concrete

by C.-T. Yu, A.S. Kobayashi and N.M. Hawkins

ABSTRACT—A hybrid experimental-numerical procedure, involving moiré interferometry and dynamic finite-element analysis, was used to analyze rapid crack growth in an impact loaded three-point-bend concrete specimen with an offset straight precrack. The dissipated energy rates in the fracture process zone (FPZ), which trails the rapidly extending crack, and in the frontal FPZ ahead of the crack tip, the kinetic-energy rate and energy-release rate were computed. The results showed that while the trailing FPZ was the dominant energy dissipation mechanism, much of the released energy was converted to kinetic energy in the fracturing concrete specimen.

Introduction

When a concrete structure, such as a runway pavement, is subjected to repeated low velocity impacts, a mode I crack which initially extends vertically from the bottom tension surface, will kink after passing through the reinforcing bars and then propagate in an apparent mixed mode I and II fracture. This failure pattern, which is described by concrete experts as diagonal tension failure, has been studied in the stable 'static' crack-growth mode by many researchers.[1-6] However, corresponding studies for mixed mode I and II concrete fracture under impact loading are yet to appear in the literature. Further, the literature is also abundant with papers on dynamic mode I failure of concrete.[7-9] But only a few papers incorporate true dynamic analysis into their data-reduction procedures.[10-12]

The factors that provide the energy-dissipation mechanism associated with concrete fracture are another little explored subject in failure studies of concrete. In contrast to the situation for metal fracture, concrete lacks the crack-tip plastic zone but dissipate some of the released strain energy through microcracking surrounding the crack tip. For concrete, surface energy along the trailing crack surface thus becomes a possible energy sink for the energy released by the fracture process. Such effect reverts fracture mechanics for concrete back to Griffith's original postulate for his global energy balance. By coincidence, recent studies of the fracture process associated with the newly created fracture surface in concrete have been inadvertently addressing the contribution of surface energy without specific reference to the associated energy dissipation. An exception is the authors' and their colleagues' recent FPZ studies where the energy dissipated in the FPZ, which trails the crack tip, was quantified for static and dynamic mode I fracture.[12-14] The salient findings in this study were that the crack-closing stress versus crack-opening-displacement relation appears to remain constant and that the energy dissipated in the trailing fracture process zone (FPZ) was a major energy sink in the fracture process of concrete.

The existence of a fracture process zone (FPZ), which trails the tip of a stably extending crack during concrete fracture, was first proposed by Hillerborg and his coworkers.[15] The associated energy dissipation in a concrete fracture specimen under mixed mode I and II loading have been studied by Guo *et al.*[6] using different FPZ constituency modeling. The constitutive equations, which governed the fracture process zone, were represented in terms of the crack-closing stress (CCS), due to FPZ, versus crack-opening displacement (COD) and the crack-shearing stress (CSS) due to aggregate interlocking, versus crack-sliding displacement (CSD). An increase in CCS over the CCS for pure mode I loading[14] in the presence of aggregate interlocking was related, thus indicating that crack bridging was influenced by friction and therefore an interaction existed between the CCS-COD and CSS-CSD relations. As a result, the dissipated energy rate in the fracture process zone also increased with increased interlocking force despite the fact that the kinked crack propagated primarily as a mode I fracture.

C.-T. Yu (SEM Member) is Post Doctoral Research Associate, and A.S. Kobayashi (SEM Fellow) is Professor, University of Washington, Department of Mechanical Engineering, FU-10, Seattle, WA, 98195. N.M. Hawkins is Professor and Head, Department of Civil Engineering, University of Illinois-Urbana, IL 61801-2297.

Paper was presented at the 1993 SEM Spring Conference on Experimental Mechanics held in Dearborn, MI on June 11.

Original manuscript submitted: September 14, 1992. Final manuscript received: April 15, 1993.

TABLE 1—AVERAGE GRADATION OF AGGREGATE

Sieve Size	No. 4	No. 8	No. 16	No. 30	No. 50	No. 100
Percent Left	1.50	15.79	28.87	43.88	78.54	97.50

TABLE 2—CONCRETE MIX PROPORTION BY WEIGHT

Cement	Sand	Gravel	Water
1.0	3.0	2.0	0.4-0.5

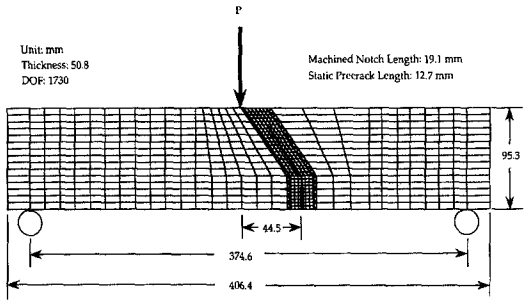

Fig. 1—Two-dimensional finite-element model of concrete specimen

Subsequent analysis by Guo[16] showed that the CCS versus COD relation varied with the development of the FPZ and that the effect of mixed-mode loading was to increase the crack-closing stress (CCS) without generating any crack-sliding resistance. In this analysis, the crack-shearing stress (CSS) was considered negligible since the topological resistance to crack sliding should vanish once the protusions are sheared. In the very vicinity of the crack tip where the CSD is nearly zero, however, CSS should exist and through increase friction it should increase the CCS. Similar conclusions were reached by Ingraffea and Panthaki[2] and Liaw *et al.*[17]

In this paper, an extension to dynamic loading of Guo's recent work on the analysis of the mixed mode I and II fracture process zone in concrete is presented.

Method of Approach

Three-point bend specimens with an off-set single-edge notch have been used by Jenq and Shah[18] to determine the crack initiation angles and peak loads. In this study, three-point-bend specimens were first statically precracked under mode I loading and then were impacted in an off-set drop weight tower. The precrack method is similar in concept with that of Hillerborg *et al.*[19] The three-point-bend specimens were instrumented with both strain gages and moiré interferometry. A hybrid experimental-numerical procedure was used to analyze the resultant data. A brief description of the experimental and numerical procedures is given in the following.

Specimen

The configuration of the three-point-bend specimen is shown in Fig. 1. Twenty specimens were made using steel molds, high early strength Portland cement, a local sand and a local coarse aggregate of 6.4-mm maximum size. Tables 1 and 2 show the aggregate gradation and the concrete-mix proportions used for this study. The concrete tensile strength, f_t, at the time of the test was estimated by $f_t = 0.54\sqrt{f_c'}$ MPa, where f_c' is the compressive strength obtained from compression testing of 150-mm diam × 300-mm length cylinders. The resultant f_t was 3.14 MPa.

A shallow notch of 0.3-mm width and 19.1-mm depth was machined in the bottom of the specimen. A unidirectional moiré diffraction grating, which yielded either the horizontal or the vertical displacements in a field of 95 × 95 mm, of 600 ℓ/mm[20] was applied to one side of the specimen. The initial machined crack was then extended by stable crack growth for about an additional 13-mm depth by subjecting the specimen to three-point-bend loading by placing the machined notch in the center of the beam span. This precracking of the specimen was conducted in the moiré interferometry setup in order to determine the crack-tip location.

Test Procedure

After precracking, mixed-mode loading was applied by rearranging the loading points so that the notch was offset from the loading point by 44.5 mm as shown in Fig. 1. The test procedure consisted of impacting the specimen in a small drop weight tower with an impactor of 10 kg from a height of 400 mm. The impact load and load-line displacement were measured by a load cell and a displacement capacitor transducer, respectively. With this impact loading, the crack kinked and propagated diagonally towards the load point.

Four or eight sequential photographs of the transient moiré fringe patterns, which represent the horizontal dis-

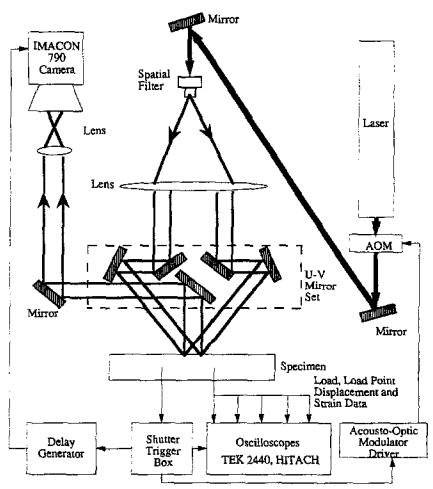

Fig. 2—Test setup for dynamic concrete tests

placements in the fracturing concrete specimen, were recorded by an IMACON 790 ultra-high-speed camera, with a fixed exposure time of 2 μs and a framing rate of 100,000 frames/s. Figure 2 shows a schematic of the test setup. The total fracture event, which lasted about 1.5 ms, was obtained by assembling a composite record of six dynamic tests on identical fracture specimens for which varying time delay was used in triggering the ultra-high-speed camera.

Due to the limited resolution of the MACON 790 camera, the vertical and horizontal displacement fields could not be recorded simultaneously on the same photograph as had been done previously.[21] Vertical displacement fields were determined from the dynamic moiré fringe patterns obtained from separate dynamic fracture tests of three identical specimens with identical loading conditions. The crack-opening and sliding displacements along the initial and kinked diagonal crack were then determined from the horizontal and vertical displacement fields through local coordinate transformation.

Numerical Procedure

An elastodynamic finite-element code was used in its propagation mode[22] to determine the CCS versus COD relation. An assumed CCS versus COD relation, together with the applied load and support boundary conditions, were iterated until they provided CODs which coincided with their measured counterparts. Figure 3 shows a typical flow chart of this iterative computation. The work done by the CCS acting on the COD for a unit crack extension was taken as the energy dissipation rate in the FPZ. The energy-release rate, kinetic-energy rate and external-work rate were computed directly from the differences in the corresponding quantities prior to and after extending the crack one finite-element nodal distance.

Results

The loading histories and crack paths, respectively, are shown in Figs. 4 and 5 for the mixed-mode dynamic concrete fracture tests. The results of the 15 different specimens are in good agreement with one another given the heterogeneity of the concrete's aggregates and their distribution as well as the inherent variability in the concrete due to slight differences in curing conditions. These agreements also justify the use of the results from multiple specimen tests to construct the complete histories of horizontal and vertical displacement fields associated with rapid and kinked crack extension in these concrete specimens. The averaged loading history and crack path, as indicated in these two figures, were used as input boundary conditions for the numerical modeling.

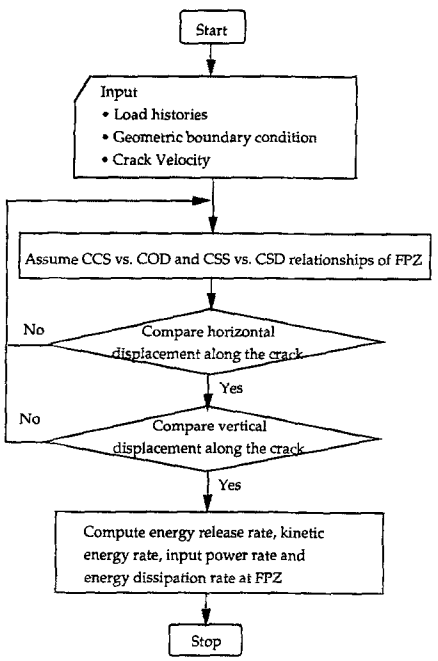

Fig. 3—Flow chart for inverse analysis

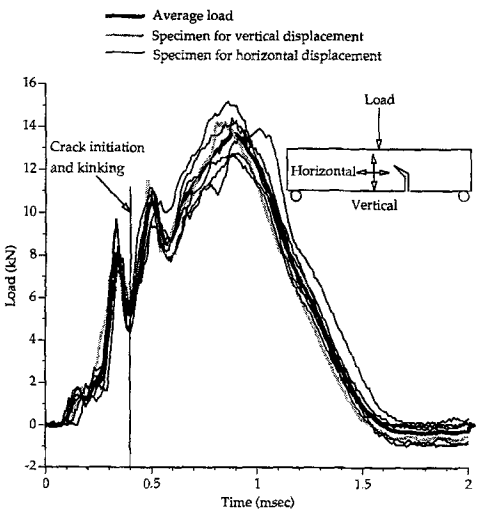

Fig. 4—Loading histories of mixed-mode dynamic concrete fracture tests

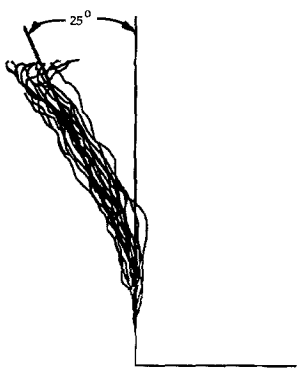

Fig. 5—Mixed-mode crack paths

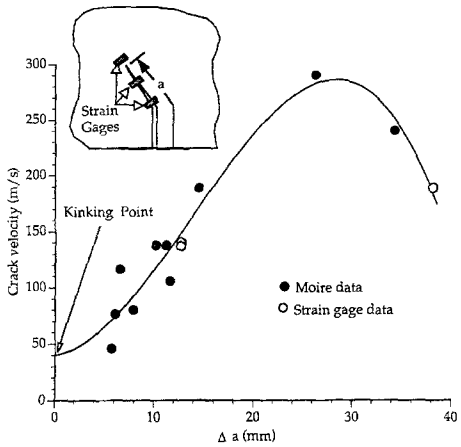

Fig. 6—Crack velocities obtained from moiré interferometry and strain gages. Δa is measured from the precrack tip

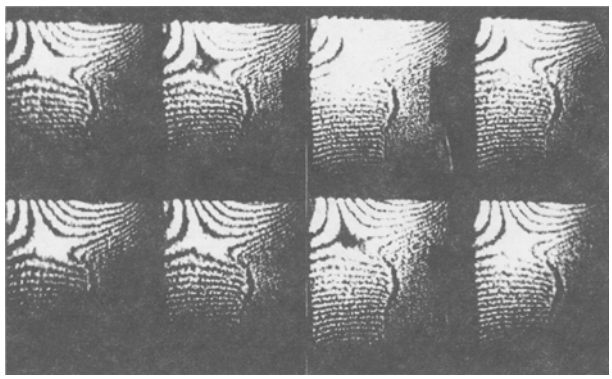

Fig. 7—Sequence of moiré patterns associated with horizontal displacement; Specimen MB2-4

Figure 6 shows the crack velocity variations with the instantaneous crack extension, Δa, where the crack length a is the length measured along the entire kinked crack path. The crack velocity reached a maximum after kinking and then decelerated as it approached the compression side of the three-point-bend specimen. The crack velocities obtained from the moiré pattern and the strain-gage readings were somewhat scattered along the same curve. The curve-fitted values for crack velocity shown in Fig. 6 were used in the numerical analysis.

Typical sequences of horizontal and vertical moiré interferometry patterns associated with the mixed mode I and II crack extensions are shown in Figs. 7 and 8, respectively. The dark square in the picture is a 25.4-mm long target used for length calibration. The sequences of horizontal and vertical displacements along the crack in Figs. 9 and 10, respectively, are associated with rapid crack extension and obtained from the moiré patterns. The coordinate, ℓ, represents the distance from the crack mouth along the kinked crack. ℓ is equal to the crack length, a, at the crack tip. The computed horizontal and vertical displacements along the crack in Figs. 11 and 12, respectively, were generated using the CCS versus COD relation of Fig. 13. Overlays of Figs. 9 and 11 and Figs. 10 and 12 are in qualitative and quantitative agreement with each other.

Figures 14 and 15 depict sequences of COD and CSD distributions, respectively, which were computed from the horizontal and vertical displacements by a coordinate transformation. The relatively constant CSD for the length

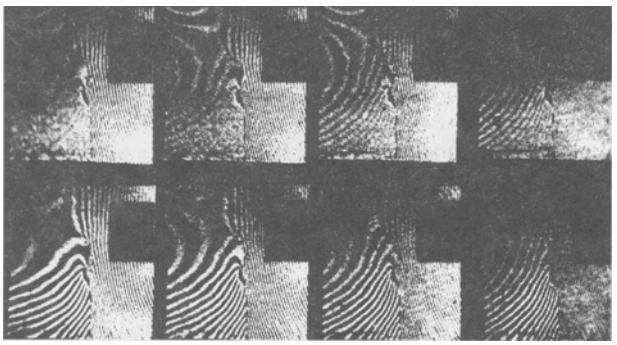

Fig. 8—Sequence of moiré patterns associated with vertical displacement; Specimen MB2-20

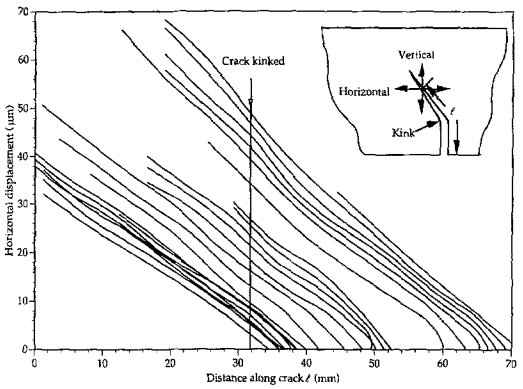

Fig. 9—Measured horizontal displacement along the crack of mixed-mode dynamic concrete fracture

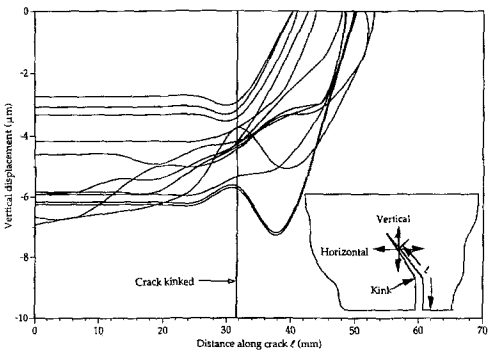

Fig. 10—Measured vertical displacement along the crack of mixed mode dynamic concrete fracture

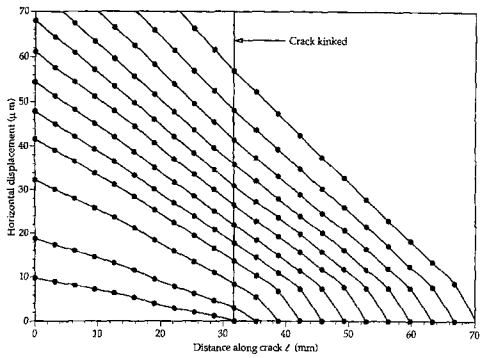

Fig. 11—Computed horizontal displacement along the crack of mixed-mode dynamic concrete fracture

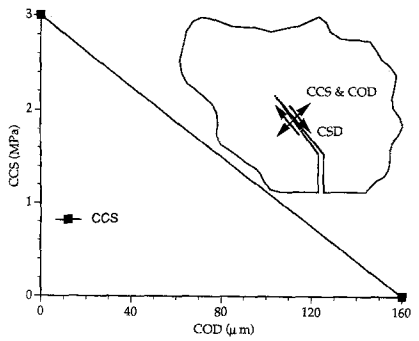

Fig. 13—Crack-closure stress and crack-opening displacement relation

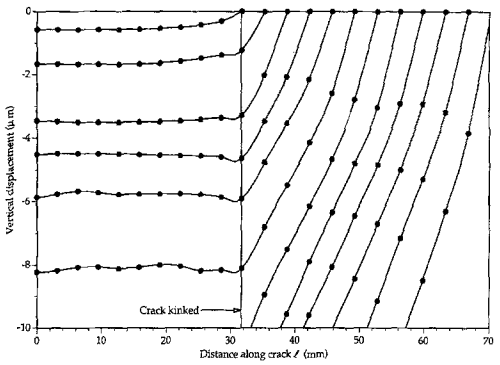

Fig. 12—Computed vertical displacement along the crack of mixed–mode dynamic concrete fracture

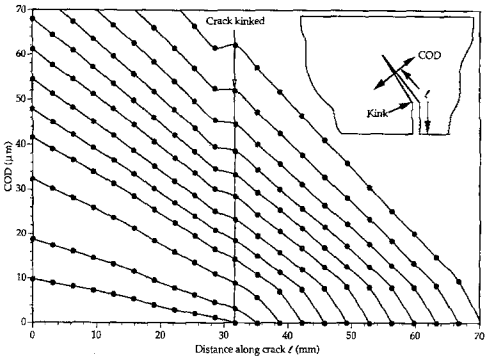

Fig. 14—Crack-opening displacement along the crack of mixed-mode dynamic concrete fracture

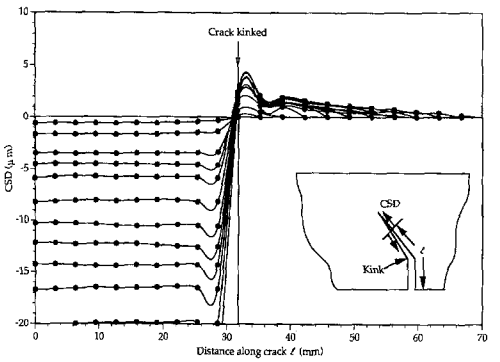

Fig. 15—Crack-sliding displacement along the crack of mixed-mode dynamic concrete fracture

of the initial straight crack indicates that the two free corners at the crack mouth of the single-edge-notch specimen are displacing relative to each other as a rigid body and are shear strain free.

Changes in energy partition with a rapid and kinked crack extension are shown in Fig. 16. Unlike the situation for somewhat ductile materials,[23] the kinetic energy is relatively large and is more characteristic of the situation for brittle materials. Figure 17 presents the energy rates obtained from Fig. 16. The small difference between energy rate dissipated along the FPZ and the energy-release rate is probably the contribution from microcracking ahead of the propagating crack.

Discussion

Figure 18 shows the load versus load-line displacement curves for FEM models with and without the computed FPZ, respectively. A comparison of the two curves shows that the load-carrying capacity is increased in the presence of a FPZ.

One piece of information missing from the foregoing discussion is the variations in the mode I and II dynamic stress-intensity factors, $K_I dyn$ and $K_{II} dyn$, with crack extension. While the static stress-intensity factors were easily determined from the superposition of two elastic states associated with the fracture specimen without the FPZ and the unloaded fracture specimen with the FPZ, respectively, no comparable solution procedure exists for the dynamic propagating crack with a FPZ. The varying $K_I dyn$, and presumably $K_{II} dyn$, with crack velocity may be of academic interest since ample experimental evidence indi-

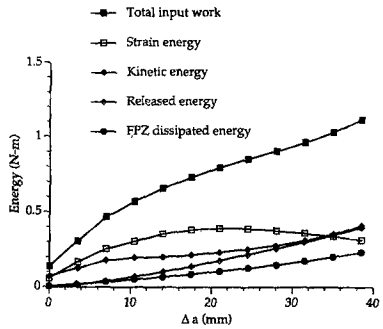

Fig. 16—Energy partition during dynamic crack propagation. Δa is measured from the precrack tip

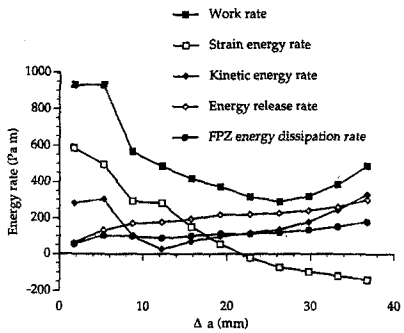

Fig. 17—Energy rates for mixed-mode dynamic concrete fracture. Δa is measured from the precrack tip

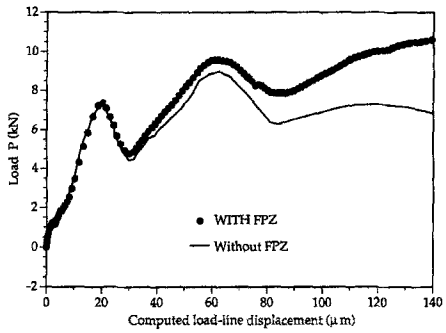

Fig. 18—Load versus computed load-line displacement curves

cates that such relations are not unique material properties.[24] The variations in K_I and K_{II} with stable crack growth, on the other hand, represent the resistance curve and are of practical interest.

Conclusions

The dynamic constitutive relations for crack bridging and interlocking in an off-set three-point-bend concrete specimens were obtained. The dominant energy-dissipation mechanism in concrete fracture is crack bridging in the fracture process zone. For the mixed-mode loading reported here the crack-propagation characteristics change gradually into those associated with mode I crack-opening deformation after kinking. The load-carrying capacity is increased in the presence of a FPZ for mixed-mode dynamic concrete fracture.

Acknowledgment

This research was supported by the U.S. Air Force Office of Scientific Research Grant IAFOSR-91-0218. The authors wish to thank Drs. T. Spencer Wu and J.C.I. Chang, AFOSR for their continuing support and encouragement during the course of this investigation.

References

1. Bazant, Z. and Pfeiffer, P.A., "Test of Shear Fracture and Strain-Softening in Concrete," 2nd Symp. on the Interaction of Non-Nuclear Munitions on Structures, Panama City Beach, FL, 254-264 (1985).

2. Ingraffea, A.R. and Panthaki, M.J., "Shear Fracture Tests of Concrete Beams," Finite Element Analysis of Reinforced Concrete Structures, Tokyo, 151-73 (1986).

3. Van Mier, J.G.M., Schlangen, E. and Nooru-Mohamed, M.B., "Shear Fracture in Cementitious Composites, Part I: Experimental Observations," Fracture Mechanics of Concrete Structures, ed. Z. Bazant, Elsevier Applied Science, 659-670 (1992).

4. Swartz, S.E. and Taha, N.M., "Mixed Mode Crack Propagation and Fracture in Concrete," Eng. Fract. Mech., **35**, *137-44 (1990).*

5. Reinhardt, H.W., Cornelissen, H.A.W. and Hordjik, D.A., "Mixed Mode Fracture Tests on Concrete," Fracture of Concrete and Rocks, ed. S.P. Shah and S.E. Swartz, Springer, 119-130 (1990).

6. Guo, Z.K., Kobayashi, A.S. and Hawkins, N.M., "Mixed Mode Concrete Fracture - An Experimental Analysis," Fracture Mechanics of Concrete Structures, ed. Z. Bazant, Elsevier Applied Sciences, 695-700 (1992).

7. Reinhardt, H.W., "Strain Rate Effects on the Tensile Strength of Concrete as Predicted by Thermodynamics and Fracture Mechanics Model," Cement Based Composites: Strain Rate Effects on Fracture, ed. S. Mindess and S.P. Shah, Material Research Society, 1-13 (1986).

8. Shah, S.P. and John, R., "Rate-sensitivity of Mode I and Mode II Fracture of Concrete," ibid. loc. cit., 21-37.

9. Bazant, Z. and Gettu, R., "Determination of Nonlinear Fracture Characteristics and Time Dependence From Size Effect," Fracture of Concrete and Rock; Recent Developments, ed. S.P. Shah, S.E. Swartz and B. Barr, Elsevier Applied Science, 549-565 (1989).

10. Ross, C.A., Kuennen, S.T. and Tedesco, J.W., "Experimental and Numerical Analysis of High Strain-Rate Concrete Tensile Tests," Micromechanics of Failure of Quasi-brittle Materials, ed. S.P. Shah, S.E. Swartz and M.L. Wang, Elsevier Applied Science, 353-63 (1990).

11. Miyamoto, A., King, M.W. and Fujii, M., "Nonlinear Dynamic Analysis of Impact Failure Modes in concrete Structures," Fracture Mechanics of concrete Structures, ed. Z. Bazant, Elsevier Applied Science, 651-6 (1992).

12. Yon, J.-H., Hawkins, N.M. and Kobayashi, A.S., "Numerical Simulation of Mode I Dynamic Fracture of Concrete," ASCE J. Eng. Mech., **117** *(7), 1595-610 (1991).*

13. Yon, J.-H., Hawkins, N.M. and Kobayashi, A.S., "Fracture Process Zone in Dynamically Loaded Double-Cantilever Beams," ACI Materials J., **88** *(5), 470-9 (1991).*

14. Guo, Z.K., Yon, J.-H., Hawkins, N.M. and Kobayashi, A.S., "Fracture Energy Dissipation Mechanism of Concrete," to be published in Fracture Mechanics, 23rd Symp., ASTM (1992).

15. Hillerborg, A., Modeer, M., and Petersson, P. E., "Analysis of Crack Formation and Crack Growth in Concrete by Means of Fracture Mechanics and Finite Elements," Cement and Concrete Res., **6**, *773-82 (1976).*

16. Guo, Z.K., "Experimental and Numerical Characterization of Fracture Behavior of Quasi-Brittle Materials," PhD thesis submitted to Univ. of Washington (Aug. 1993).

17. Liaw, B.M., Jeang, J.L., Hawkins, N.M. and Kobayashi, A.S., "Fracture Process Zone for Mixed Mode Concrete Fracture," ASCE J. Eng. Mech., **86** (7), 1560-1579 (1990).

18. Jenq, Y. S. and Shah, S. P., "Mixed-Mode Fracture of Concrete," Int. J. Fract., **38**, 123-42 (1988).

19. Hassanzadeh, M., Hillerborg, A., and Zhou, F.P., "Tests of Material Properties in Mixed Mode I and II," RILEM Report 5, Proc. of SEM-RILEM International Conference on Recent Developments in the Fracture of Concrete and Rock, ed. S.P. Shah and S.E. Swartz, Houston, TX, June 17-19, 353-58 (1987).

20. Post, D., "Moiré Interferometry," Handbook on Experimental Mechanics, ed. A.S. Kobayashi, Prentice-Hall, 314-87 (1984).

21. Dadkhah, M.S., Wang, F.X. and Kobayashi, A.S., "Simultaneous On-Line Measurement of Orthogonal Displacement Fields by Moiré Interferometry," EXPERIMENTAL TECHNIQUES, **12**, 28- 30 (1988).

22. Kobayashi, A.S., "Dynamic Fracture Analysis by Dynamic Finite Element Analysis - Generation and Propagation Analyses," Nonlinear and Dynamic Fracture Mechanics, ed. N. Perrone and S.N. Atluri, ASME AMD-35,19-36 (1979).

23. Kobayashi, A.S., Seo, K., Jou, J.Y. and Urabe, Y., "Dynamic analyses of Homalite-100 and Polycarbonate Modified Compact Tension Specimen," EXPERIMENTAL MECHANICS, **20** (3), 73-9 (1980).

24. Kobayashi, A.S., Ramulu, M., Dadkhah, M.S., Yang, K-H.and Kang, B.S.-J., "Dynamic Fracture Toughness," Int. J. Fract., **30**, 275-85 (1986).

ERRATA

"Optimal Orientation of Flakes in Oriented Strand Board (OSB)," V. Sharma and A. Sharon, Vol. 33, No. 2 (June 1993).

The illustration labelled Fig. 8 on page 89 is incorrect. The correct Fig. 8 appears below. EXPERIMENTAL MECHANICS regrets this error and apologizes for any confusion it has caused its readers.

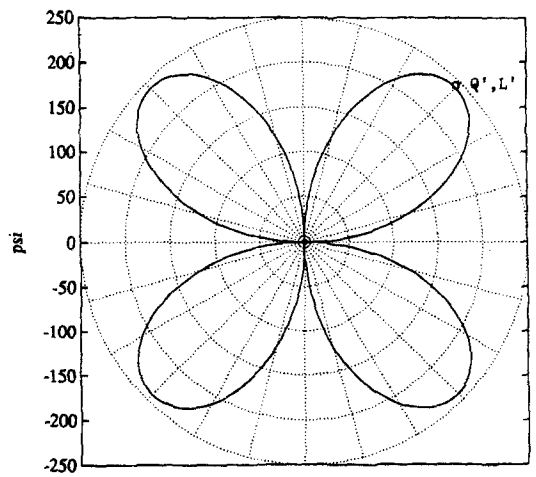

Fig. 8—Polar plot of the variation in shear stress along different directions at a point in the OSB sheet

"The Effect of Residual Stresses on Hardness Measurements," J. Frankel, A. Abbate and W. Scholz, Vol. 33, No. 2 (June 1993).

The illustration labelled Fig. 5 on page 167 is incorrect. The correct Fig. 5 appears on page 168 and is labelled Fig. 6. The correct Fig. 6 appears below. EXPERIMENTAL MECHANICS regrets these errors and apologizes for any confusion it has caused its readers.

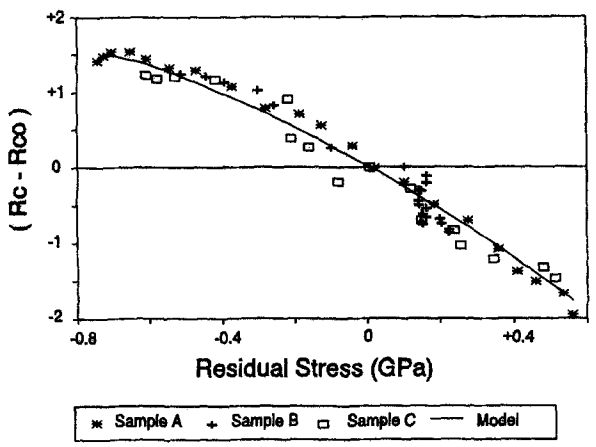

Fig. 6—Change in Rockwell *C* hardness versus residual hoop stress. The solid line represents the model fit for $\alpha = 0.18$